

This is a post-print (final draft post-refereeing). Published in final edited form as:

Bermúdez, H.D., Bolívar, L., Arz, J. A., Arenillas, I., Gilabert, V., DePalma, R., Philips, G., De Palma, M., Bermúdez, D., Gómez, C. y Cui, Y. (2025): *The sedimentological signature of impact spherules and its relation to ejecta transport mechanisms during the Chicxulub asteroid impact (Cretaceous/Paleogene boundary)*. Journal of South American Earth Sciences, 153, 105338, 1-11.

DOI: 10.1016/j.jsames.2024.105338.

Published online 03 January, 2025

Available in: <https://www.sciencedirect.com/science/article/pii/S0895981124005601?via%3Dihub>

1 The sedimentological signature of impact spherules and its
2 relation to ejecta transport mechanisms during the Chicxulub
3 asteroid impact (Cretaceous/Paleogene boundary)

4 **Hermann D. Bermúdez^{1-3*}, Liliana Bolívar², José A. Arz⁴, Ignacio Arenillas⁴, Vicente**
5 **Gilbert⁴⁻⁵, Robert DePalma⁶⁻⁷, George Phillips⁸, Daniela Bermúdez⁹, Maurizia De Palma¹,**
6 **Clemencia Gómez³, Ying Cui¹**

7 *¹Department of Earth and Environmental Studies, Montclair State University, Montclair, NJ*
8 *07043, USA.*

9 *²Grupo de Investigación Paleoexplorer, 1400-37 Trexlertown Rd. PA 18062, USA.*

10 *³Departamento de Geociencias, Universidad Nacional de Colombia, Bogotá 11001, Colombia.*

11 *⁴Departamento de Ciencias de la Tierra-IUCA, Universidad de Zaragoza, E-50009 Zaragoza,*
12 *Spain.*

13 *⁵Departament de Dinàmica de la Terra i de l'Oceà, Universitat de Barcelona, E-08028*
14 *Barcelona, Spain.*

15 *⁶Department of Earth and Environmental Sciences, University of Manchester, Manchester, M13*
16 *9PL, UK.*

17 *⁷Department of Geosciences, Florida Atlantic University, Boca Raton, FL 33431, USA.*

18 *⁸Mississippi Museum of Natural Science, Conservation & Biodiversity Section, Jackson, MS*
19 *39202, USA.*

20 *⁹Science and Technology School, Environmental Sciences for Sustainability, Ie University, C.*
21 *Cardenal Zúñiga, 12, Segovia, Castilla y Leon 40003, Spain.*

22 **Corresponding author: bermudezh@montclair.edu*

23 **ABSTRACT**

24 The Chicxulub impact is the most likely cause of the Cretaceous/Paleogene boundary
25 (KPB) mass extinction and the only impact event in Earth's history with a globally traceable
26 ejecta bed. Although the impact spherules are thought to represent molten or vaporized material,
27 precise genesis and transport mechanisms remain underconstrained. Here, we show that the
28 morphology, size, internal structure, and distribution of the spherules within the KPB deposits
29 are related to origin and transport processes. The study of thousands of spherules from KPB
30 deposits in Colombia, the USA, and Spain has revealed the presence of three fractions related to
31 three different distribution processes, each with a distinctive sedimentological signature. The
32 coarser fraction ("aspergo deposit," from the Latin *aspergo*, meaning splash) comprises
33 rotational and agglutinated/irregular forms (size > 2mm) containing abundant vesicles, unmelted
34 inclusions, and schlieren, implying an origin from molten materials and transport following
35 ballistic trajectories. The intermediate fraction ("pyrocloud deposit" from the Greek *pyr*, meaning
36 fire) represents a mixture of molten and condensed droplets, including spheres, rotational, and
37 agglutinated/irregular forms (size 0.3 - 2 mm), transported by the rapid expansion of a fast-
38 moving, high-temperature turbulent cloud. The globally distributed finer fraction ("fireball
39 layer") is composed exclusively of spheres (size < 0.3 mm) condensed from a vapor plume after
40 the Chicxulub impact. These observations provide valuable insights into ejecta distributions
41 during massive asteroid impacts and enhance our understanding of the Chicxulub impact and its
42 aftermath.

43

44 **Keywords:** Chicxulub, Cretaceous/Paleogene boundary, impact spherules, morphology, ejecta
45 distribution.

46

47 **1. Introduction**

48 Asteroid impacts are frequent events in the evolution of the Solar System. As a result,
49 impact craters are the most common type of landform in the planetary bodies that compose it
50 (Koeberl, 2002; Simonson and Glass, 2004). While the number of well-documented asteroid
51 impacts on Earth is relatively low, since the Earth's crust is highly dynamic, these events have
52 left a deep imprint on the geological record and the evolution of life (Pierazzo and Artemieva,
53 2012; Schmieder and Kring, 2020; Osinski et al., 2022;). During the earliest stages of high-
54 velocity impact events, large volumes of vaporized, molten, and crushed material are expelled
55 over large areas, forming an ejecta layer that thins away from the crater (Melosh, 1989; Kring
56 and Durda, 2002; Glass and Simonson, 2012; Osinski et al., 2022). Ejecta deposited less than 2.5
57 times the impact crater diameter is called proximal ejecta (5 times according to Koeberl, 2002);
58 materials ejected beyond that distance are called distal ejecta (Glass and Simonson, 2012).

59 Glass produced by melting during impact events is called impact glass or impactite
60 (Koeberl, 1986) and is an important component of the ejecta layers. There is no clarity or
61 agreement on how to describe ejecta composed mainly of impact glass, as there are different
62 terms according to their size, composition, and origin (Rieihart, 1958; Stöffler, 1984; Koeberl,
63 1986; Glass and Burns, 1988; Koeberl, 1992; Koeberl, 1993; Koeberl, 2002; Elkins-Tanton et
64 al., 2003; Glass and Simonson, 2011; Glass and Simonson, 2012; Glass, 2016; Macris et al.,
65 2018). Nonetheless, we can consider that as it cools down, the ejected material can form large
66 glass bodies centimeters in size or larger, called tektites, and smaller glass bodies, called impact
67 spherules (Glass and Simonson, 2012; Glass, 2016). According to the original description (Suess,
68 1900), tektites, from the Greek *τήκτος* - *tektos*, meaning molten, are melt droplets composed
69 entirely of macroscopically homogeneous glass (Rieihart, 1958; Koeberl, 1986; Glass and Burns,

70 1988; Koeberl, 2002; Glass, 2016). According to the size (Glass and Simonson, 2013), it is
71 possible to subdivide the tektites into micro (<1 mm diameter), mini (1-10 mm diameter), and
72 macrotektites (>10 mm diameter). Impact spherules (*i.e.*, spheres or rounded bodies up to a few
73 millimeters in size) are glassy spherules formed due to extraterrestrial impacts and represent a
74 significant volume of the distal ejecta. By composition (Glass and Simonson, 2012; Glass, 2016),
75 it is possible to define two types of impact spherules: (1) microtektites, which do not contain
76 primary microlites, and (2) mikrokrystites (Glass and Burns, 1988), which have partly
77 crystallized and contain microlites. According to their original definition, microtektites are
78 melted in origin (Koeberl, 2002), although some authors (e.g., Elkins Tanton et al., 2002)
79 considered it predominantly condensate droplets. In turn, it is assumed that mikrokrystites
80 correspond to condensed droplets (Johnson and Melosh, 2012; Belza et al., 2017; Goderis et al.,
81 2021), although depending on the composition of the melt and temperature history, microtektites
82 can form from plume condensate droplets and mikrokrystites can be formed from melt ejecta
83 droplets (Glass and Simonson, 2011). Most of the melted ejecta spherules are microtektites, and
84 most of the spherules formed from condensate droplets are mikrokrystites.

85 Impact spherule beds form rapidly and can be distributed regionally or globally (e.g., the
86 Cretaceous/Paleogene boundary - KPB); therefore, they represent excellent time-stratigraphic
87 markers (Montanari and Koeberl, 2000; Simonson and Glass, 2004; Glass and Simonson, 2012;
88 Vajda and Bercovici, 2014). The Chicxulub impact is an ideal case study since it is the only
89 recognized impact event on Earth that preserved a globally traceable ejecta layer (Smit, 1999;
90 Claeys et al., 2002; Schulte et al., 2010; Artemieva and Morgan, 2020; Goderis et al., 2021;
91 Gulick, 2025), and it is the most likely cause of the KPB mass extinction (Arz et al., 2004;
92 Arenillas et al., 2006; Molina et al., 2009; Schulte et al., 2010; Morgan et al., 2022; Chiarenza

93 and Brusatte, 2023). The Chicxulub impact expelled millions of tons of molten and vaporized
94 materials in an impact plume and ejecta curtain, constituting, once settled, the global KPB
95 deposits (Artemieva et al., 2017; Gulick et al., 2019; Morgan et al., 2022).

96 The global record of the KPB has been extensively studied since the discovery of the
97 Chicxulub crater (Hildebrand et al., 1991). Overall, the stratigraphy and thickness of the KPB
98 deposits vary with distance from the crater (Schulte et al., 2010), although local conditions and
99 accommodation may affect thickness (Gulick, 2025). In proximal sites (< 1,000 km from
100 Chicxulub's crater), the stratigraphy of the KPB deposits is complex, and the thickness varies
101 depending on the amounts of remobilized sediments and subsequent re-deposition by several
102 mechanisms such as impact-triggered tsunamis, submarine landslides, sediment fluidization and
103 liquefaction, slumping or gravity flows (e.g., Bralower et al., 1998; Smit, 1999; Arz et al., 2001;
104 Soria et al., 2001; Schulte et al., 2012; Denne et al., 2013; Sanford et al., 2016; Gulick, 2025). In
105 the Gulf of Mexico and the Caribbean, the KPB deposits are generally fining-upward
106 sedimentary successions with a metric or decametric thickness, although they can exceed
107 hundreds of meters (Sanford et al., 2016; Christeson et al., 2021; Arz et al., 2022). For
108 intermediate sites (1,000 - 5,000 km), the thickness of the KPB deposits ranges from centimeters
109 to decimeters, showing a distinct dual-layer stratigraphy (Smit, 1999; DePalma et al., 2019;
110 Gulick, 2025) in which the lower part is similar to spherule beds in proximal sites, while the
111 upper part is comparable to the global distal ejecta layer (Artemieva and Morgan, 2009). Distal
112 sites (> 5,000 km) record a thin (2 - 4 mm) ejecta layer known as the "fireball layer" (Bohor,
113 1990; Hildebrand and Boynton, 1990). The fireball layer is typically 2 to 4 mm thick and is
114 characterized by abundant impact spherules presumably formed from vaporized target rock and
115 meteorite materials, shocked minerals, and sediments enriched in platinum-group elements

116 (Johnson and Melosh, 2012). Importantly, this layer establishes a crucial temporal horizon that
117 precisely links the Chicxulub impact to the KPB (Artemieva and Morgan, 2009; Belza et al.,
118 2017; Claeys et al., 2002; Goderis et al., 2021). Nevertheless, the processes and mechanisms
119 forming and transporting the ejecta to distal positions remain underconstrained. Some authors
120 argue that the fireball layer represents shocked, metamorphosed mineral grains and condensed
121 droplets from a vapor plume traversing the globe ballistically (Kring and Durda, 2002; Johnson
122 and Melosh, 2012; Belza et al., 2017). This idea conflicts with three-dimensional numerical
123 models and the stratigraphic record, as a purely ballistic distribution scenario is insufficient to
124 explain a global boundary layer due to disparities in KPB bed thickness, ejection velocities, and
125 the required volume of vaporized materials (Artemieva and Morgan, 2020).

126 Recognizing the importance of integrating physical evidence to understand the processes
127 governing the formation and distribution of ejecta materials during the Chicxulub impact, we
128 analyzed impact spherules from four high-fidelity KPB sites in North and South America and
129 Western Europe. Our findings demonstrate that geological and sedimentological observations are
130 key tools to provide direct, robust, and accurate information about ejecta features and the relation
131 to distribution mechanisms. Here, we conduct a detailed sedimentological analysis of impact
132 spherules from sites located at different distances from the crater to explore the connection
133 between the spherule morphology, size, internal structure, and distribution within the KPB bed
134 and the origin and potential transport mechanisms. This analysis sheds light on the processes that
135 govern the global transport of Chicxulub-derived ejecta and will help improve recent ejecta
136 distribution numerical models during massive asteroid impacts, allowing a better understanding
137 of its influence on climatic and environmental changes at regional and global scales.

138

139 **2. Geological setting**

140 The samples studied were obtained from the bed representing the KPB in outcrops from
141 Wahalak Creek, Mississippi, USA; Tanis, North Dakota, USA; Gorgonilla Island, Colombian
142 Pacific; and Zumaia, Basque Country, northern Spain (Fig. 1). According to paleogeographic
143 maps (Scotese, 2021), at the time of the KPB, the sites were located approximately 1,500 km
144 north, 3,000 km north, 3,000 km south, and 7,000 km east of the Chicxulub crater, respectively.

145 The ~2-m-thick bed representing the KPB in Wahalak Creek (Fig. 2 A-C) corresponds to
146 channelized deposits of sandstones and conglomerates with abundant macrofossils and impact
147 spherules, interpreted as tsunami deposits, interbedded between the Danian Clayton Formation
148 and the Maastrichtian Prairie Bluff Chalk Formation (Larina et al., 2016; Witts et al., 2018;
149 Sosa-Montes de Oca et al., 2024). Due to poor preservation and limited exposure, small
150 spherules from the upper part of these strata, which include fine sandstones and mudstones that
151 potentially preserve the fireball layer, were not analyzed.

152 The ~ 1.3-m-thick bed representing the KPB in Tanis (Fig. 2 D-F) shows a normally
153 graded sequence of coarse sandstone to siltstone/claystone that includes impact spherules and a
154 mass death assemblage of diverse marine and terrestrial fossils. The ejecta-bearing sediments
155 were emplaced by two massive impact-triggered surges during the first hours after the impact
156 (DePalma et al., 2019; LeVeque et al., 2024). Evidence supporting the link to the Chicxulub
157 impact is based on a geochemical match with unmelted Chicxulub glass found in other locations
158 and a $^{40}\text{Ar}/^{39}\text{Ar}$ age of unmelted glass cores from altered spherules. This age is well aligned with
159 Chicxulub melt-rock and spherules from different sites (DePalma et al., 2019). This bed overlies
160 point bar deposits typical of the Hell Creek Formation and is overlain by a 1-2-cm-thick clay-
161 altered layer (not studied here) corresponding to a smectitic tonstein, comparable to the "fireball

162 layer," enriched with spherules, shocked minerals, iridium, and other impact-derived materials
163 (DePalma et al., 2019) representing the settling of fine debris long after the Chicxulub impact
164 (Goderis et al., 2021).

165 The KPB bed at Gorgonilla Island (Fig. 2 G-I) corresponds to a normally graded ~2-cm-
166 thick sequence of incredibly preserved glass spherules (Bermudez et al., 2016; Bermúdez et al.,
167 2018), with an $^{40}\text{Ar}/^{39}\text{Ar}$ age of 66.051 ± 0.031 Ma (Renne et al., 2018). Gorgonilla Island
168 impact spherules are virtually intact (up to 90% preserve the original glass and are not altered to
169 clay minerals as other sites), representing the most pristine Chicxulub impact spherules known to
170 date. The spherule-rich bed is interbedded between rhythmic intercalations of litharenites and
171 tuffaceous marls, interpreted as deep-sea marine turbidites deposits (Bermudez et al., 2016;
172 Bermúdez et al., 2018).

173 The KPB bed at Zumaia (Fig. 2 J-L) corresponds to a millimeter-thick red layer with
174 impact spherules, overlain by a 9-cm-thick blackish claystone bed, interbedded between the
175 Maastrichtian Zumaia-Algorri Formation reddish marls and the Danian Aitzgorri Formation red-
176 pink marly limestones deposited in a middle bathyal setting (Gilabert et al., 2022).

177

178 **3. Materials and methods**

179 Considering that this contribution is focused on the study of morphological and
180 morphometric aspects of Chicxulub impact-related droplets, here we use the generic term
181 "impact spherules" (Glass, 2016) to describe the vitreous and altered droplets preserved in
182 intermediate to distal deposits of the KPB. No distinctions are made regarding spherules' size,
183 origin, or composition. KPB beds were gently disintegrated, and individual spherules were
184 picked by hand under a Zeiss Stemi 508 Stereo Microscope in the Paleoclimatology lab at

185 Montclair State University. From the Wahalak Creek KPB bed, about 500 g of rock was
186 disaggregated to obtain about 1,000 individual spherules, from which 900 were selected for
187 morphological analysis. For the Tanis samples, approximately one cubic meter of sediment from
188 the lower-middle graded surge pulse (unit 2) was disaggregated with water and a 0.5% hydrogen
189 peroxide solution before passing through nested sieves. Spherules were hand-picked from the
190 residuum, which consisted of coarse material and agglomerated fine sediment that remained after
191 sieving, obtaining 200 individual spherules for morphological analysis. From the Gorgonilla
192 Island KPB bed, about 200 g of rock was disaggregated to obtain over 5,000 individual
193 spherules, from which 2,000 were randomly selected for morphological analysis. From the
194 Zumaia KPB bed, about 100 g of rock was disaggregated to obtain about 300 individual
195 spherules, from which 225 spherules were randomly selected for morphological analysis.
196 Spherules were categorized using a morphological classification scheme based on previously
197 published mathematical models (Fig. 3), numerical simulations, and experimental findings
198 (Elkins-Tanton et al., 2003; Stauffer and Butler, 2010; Butler et al., 2011; Baldwin et al., 2015).

199 The photographic record of representative spherules was made using a 5MP Zeiss
200 Axiocam 208 color camera. To provide further information on the morphological features of the
201 impact spherules, additional photos of polished sections (Gorgonilla Island section) or individual
202 spherules (Gorgonilla Island and Zumaia sections; Mississippi spherules are deemed too altered
203 and unsuitable for SEM images) were taken under a Quanta FEG 650 scanning electron
204 microscope (SEM) at the Department of Geosciences at the Swedish Museum of Natural History,
205 Stockholm, Sweden (Gorgonilla spherules) and a Zeiss MERLIN FE-SEM in the Electron
206 Microscopy Service of the Universidad de Zaragoza, Spain (Zumaia spherules).

207 For morphological classification, three categories were considered: 1) spheres, 2)
208 rotational forms, and 3) agglutinated-irregular forms. Using models starting with spherical
209 shapes, Fig. 3 illustrates the geometrical parameters and a new model that groups the shapes
210 experimentally obtained by subjecting liquid droplets to rotation (Elkins-Tanton et al., 2003;
211 Stauffer and Butler, 2010; Baldwin et al., 2015). The conditions necessary to obtain those shapes
212 are explained below. Although our findings demonstrate the formation of all these rotational
213 shapes within the spherules resulting from the Chicxulub impact, a detailed analysis of each
214 morphology is beyond the scope of this research. Finally, the agglutinated-irregular forms
215 include all morphologies resulting from the agglutination or irregular deformation of pre-existing
216 spheres or rotational forms.

217 We consider three categories for size classification: 0.1 – 1 mm, 1 – 10 mm, and 10 – 100
218 mm size fractions. For the 0.1 – 1 mm size fraction, we count the total occurrence and proportion
219 of the three shape categories every 0.1 mm increment. For the 1 – 10 mm size fraction, we
220 estimate the percent of these shapes every 1 mm increment. For sizes larger than 10 mm, every
221 10 mm increment is considered.

222

223 **4. The physics of the impact spherules**

224 Impact spherules correspond to glassy droplets formed during asteroid impacts
225 (Simonson and Glass, 2004; Johnson and Melosh, 2012). Impact spherules include diverse
226 shapes that depend on the processes occurring during and after the flight before they undergo
227 cooling and solidification (Simonson and Glass, 2004; Stauffer and Butler, 2010). The shape is
228 related to the physics of liquid spinning droplets (bodies of revolution) following a transitional
229 sequence that begins with a sphere and deforms through viscous fluid flow processes into other

230 shapes depending on surface tension and rotational velocity (Elkins-Tanton et al., 2003; Stauffer
231 and Butler, 2010; Baldwin et al., 2015).

232 Physical parameters govern droplet dynamics and stability of spinning, as translating
233 droplets during laboratory experiments demonstrated that moving droplets assume the form of
234 bodies of rotation if rotational speed is only 1% or more of translational speed (Elkins-Tanton et
235 al., 2003). Secondary processes (occurring during flight) include ablation, spalling,
236 fragmentation, degassing, and bubble formation, while ground impact leads to plastic flattening,
237 bending, and impact fragmentation. After landing, spalling and degassing may also occur
238 (Stauffer and Butler, 2010). Additionally, it is important to note that collisions may occur during
239 flight or at the time of deposition, deforming or causing the agglutination of one or more
240 spherules if they have not yet solidified and also potentially increasing the incidence of unmelted
241 inclusions if the fragments are appressed between the agglutinating spherules.

242 It has been experimentally demonstrated that increased dimensionless angular momentum
243 allows a sphere to progressively evolve into oblate shapes, tri-axial ellipsoids, and finally,
244 dumbbells, until unstable shapes are produced when the angular momentum is greater than 2.0,
245 including theoretical triangular unstable equilibrium shapes for values between 2.0 and 2.8
246 (Elkins-Tanton et al., 2003; Stauffer and Butler, 2010; Baldwin et al., 2015).

247 In equilibrium (when pressure and centrifugal forces are precisely in balance everywhere
248 inside the drop), the shape of a fluid drop is uniquely parameterized by the so-called Eötvös or
249 Bond number. The Bond number is a non-dimensional number defined by the quotient of the
250 gravitational forces and the forces due to surface tension (Elkins-Tanton et al., 2003; Stauffer
251 and Butler, 2010). The Bond number is described in the following equation (Eq. 1):

$$252 \quad B_0 = \rho\Omega^2 R^3 / 8\sigma. \quad (1)$$

253 Where ρ , Ω , and σ are the density, rotational frequency, and surface tension of the fluid drop.
254 The variable R represents the radius of a sphere with the same volume as the drop.
255 It has been observed that there are no centrifugal forces at zero values of B_0 (a particular case
256 when the rotational velocity is zero), and the surface tension creates perfectly spherical shapes
257 for the spherules. B_0 values up to 0.09 produce approximately oblate ellipsoids. B_0 values
258 between 0.09 and 0.31 allow both oblate ellipsoids and dumbbells. B_0 values greater than 0.31
259 allow for the development of unstable, in equilibrium, axisymmetric shapes, which become bi-
260 concave when an angular momentum of 0.5 is exceeded, and a torus's shape is achieved when the
261 B_0 value is at 0.57. Beyond 0.57, there are no equilibrium shapes, and the droplet will eventually
262 pinch off into two or more drops (Stauffer and Butler, 2010; Butler et al., 2011). Alternatively, it
263 has been proposed that based on the spin pattern and the spin rate, relatively rapid spin rates
264 allow the evolution of spheres into rods and dumbbells, eventually separating into teardrops that,
265 if maintaining sufficient fluidity, can again reach a spherical shape. At low spin rates, discs,
266 bowls, and torus shapes evolve when central thinning develops (Beyer, 1962).

267

268 **5. Results**

269 The results of the shape and size distribution of the impact spherules (Table S1, Fig. 4,
270 and Fig. 5) are based on 900, 200, 2,000, and 225 individual spherules from Wahalak Creek,
271 Tanis, Gorgonilla Island, and Zumaia, respectively. Quantities vary according to absolute
272 abundance and preservation. Only spherules from the high-energy deposits of the lower part of
273 the KPBed were studied in Wahalak Creek and Tanis. The thin deposits in the upper part of the
274 KPBed, although they include spherules, were not analyzed in this study due to poor
275 preservation.

276 Our analysis is consequent with an increase in size in the direction of the crater (Fig. 5A)
277 and reveals the occurrence of three different populations with a characteristic sedimentological
278 signature (Fig. 5B-C). Spherules larger than 2 mm do not include spheres. Spherules of
279 intermediate size (0.3 and 2 mm) involve variable proportions of spherical, rotational, and
280 agglutinated/irregular forms. Finally, spherules smaller than 0.3 mm are composed of spheres
281 only.

282

283 **5.1. Wahalak Creek**

284 At Wahalak Creek (Fig. 4G, 5A-B, and Table S1), impact spherules with sizes between
285 0.5 and 11 mm were identified. No spheres larger than 2 mm were observed. The proportion of
286 spheres increases as the size decreases until it reaches 33.3% of the population in the 0.5-0.6 mm
287 fraction. The proportion of rotational forms is variable but constitutes the most abundant
288 morphology (> 70%) in the size fraction between 1 and 5 mm, where most of the impact
289 spherules from this locality are concentrated (~88%). Rotational forms represent 100% of the
290 population at sizes > 8 mm; however, they only include a few impact spherules. In fractions with
291 sizes > 8 mm and < 1 mm, there are no agglutinated/irregular forms. The proportion of
292 agglutinated/irregular forms is variable but never exceeds 50% of the population, which occurs
293 in size fraction between 6-8 mm.

294

295 **5.2. Tanis**

296 At Tanis (Fig. 4E, 5A-B, and Table S1), impact spherules with sizes between 0.4 and 4
297 mm were observed. No spheres larger than 2 mm were observed. The proportion of spheres is
298 variable but reaches 60% of the population in the 0.3-0.4 mm fraction. The proportion of

299 rotational forms is variable but constitutes the most abundant morphology (> 70%) in the size
300 fraction between 0.4 and 2 mm, where most of the spherules from this locality are concentrated
301 (~89%). No agglutinated/irregular forms were recognized for the spherules with sizes > 4 mm
302 and < 0.9 mm. The proportion of agglutinated/irregular forms increases with the size of the
303 spherules, reaching 50% of the population in the 3-4 mm fraction.

304

305 **5.3. Gorgonilla Island**

306 At Gorgonilla Island (Fig. 4F, 5A-B, Table S1), impact spherules with sizes between 0.2
307 and 5 mm were observed. No spheres larger than 2 mm were observed. The proportion of
308 spheres increases as the size decreases until it reaches 100% of the population in the finest
309 fraction (0.3-0.4 mm). Overall, the proportion of rotational forms increases with increasing size,
310 reaching 100% in the coarsest fraction (4-5 mm fraction) and constitutes the most abundant
311 morphology (> 50%) in the size fraction between 0.8 and 3 mm, where most of the spherules
312 from this locality are concentrated (~84%). As in the Tanis section, no agglutinated/irregular
313 forms were recognized in the size fraction > 4 mm and < 1 mm. The proportion of
314 agglutinated/irregular forms is variable but never exceeds 46% of the population, which occurs
315 only in the size fraction between 2-3 mm.

316

317 **5.4. Zumaia**

318 At Zumaia (Fig. 4D, 5A-B, Table S1), impact spherules with sizes between 0.1 and 3 mm
319 were observed, and unlike the previous localities, no agglutinated/irregular forms were identified
320 in any of the documented size fractions. Notably, no spheres larger than 1 mm were detected,
321 and the proportion increases as the size fraction decreases until it reaches 100% of the population

322 in the finest fractions (< 0.3 mm). Spherical shapes constitute the most abundant morphology (>
323 85%) in the fractions between 0.2 and 0.5 mm, where most of the spherules from this locality are
324 concentrated (~90%). Overall, the proportion of rotational forms increases with increasing size,
325 reaching 100% in the coarsest fractions (> 0.7 mm); however, these sizes only include a few
326 impact spherules.

327

328 **6. Discussion**

329 Our analyses of the morphology, size, internal structure, and distribution of the impact
330 spherules within the KPB bed from spatially variable sites can provide physical evidence which
331 sheds light on the debate surrounding the transport mechanism of the Chicxulub impact ejecta
332 and its global distribution. We identify three distinct populations within the KPB deposits by
333 analyzing morphologically and morphometrically thousands of impact spherules deposited at
334 intermediate and distal distances to the north, south, and east of the Chicxulub crater (Fig. 5A-
335 B). These populations correspond to an idealized, normally graded tripartite sequence (Fig. 5C)
336 when the deposits are complete and undisturbed, as occurs in a few sites such as Gorgonilla
337 Island (Fig. 4F) or Demerara Rise (Schulte et al., 2009).

338 **6.1. Sedimentologic signature of Chicxulub-associated impact spherules**

339 The coarsest size fraction includes spherules larger than 2 mm and is composed
340 exclusively of rotational and agglutinated/irregular forms (*i.e.*, no spheres). When the KPB
341 deposits are complete and undisturbed, this population may constitute a basal deposit that we call
342 the "aspergo deposit," a new term from the Latin *aspergo*, meaning splash. Spherules from the
343 aspergo deposit were identified at all studied sites (Fig. 4 and Fig. 5), but only one was found at
344 Zumaia (Table S1).

345 The intermediate fraction (0.3 to 2 mm in size) includes spheres, rotational, and
346 agglutinated/irregular shapes and may comprise a transitional deposit that we call "pyrocloud
347 deposit," a new term from the Greek *pyr*, meaning fire. Spherules from the pyrocloud deposit
348 were identified at all sites studied (Table S1). This population has a transitional mixture of
349 relatively large spherules, similar to those of the aspergo deposit, and relatively small spherules,
350 similar to those of the fireball layer. Unlike the aspergo deposit, the large forms include
351 spherules, while the smaller ones, distinct from the fireball layer, include rotational shapes (Fig.
352 4 and Fig. 5).

353 The finest fraction (size <0.3 mm) includes only spheres (i.e., no rotational or
354 agglutinated/irregular forms) and is equivalent to the previously reported "fireball layer" from
355 European and North American localities (Smit, 1999; Molina et al., 2006; Artemieva and
356 Morgan, 2009; Belza et al., 2017). Spherules from the fireball layer were studied using samples
357 from Gorgonilla Island and Zumaia KPB sections (Fig. 4, Fig. 5, and Table S1).

358 Combined, the aspergo deposit and the pyrocloud deposit constitute the totality of the
359 spherules present in the high-energy geologically quasi-instantaneous KPB deposits (*i.e.*,
360 deposited over minutes to hours) associated with the Chicxulub impact in positions relatively
361 close to the Chicxulub crater in the Americas. Numerous authors describe these materials as the
362 bottom of a "dual stratigraphy" for the KPB bed that at the top contains the globally distributed
363 fireball layer (Smit, 1999; Artemieva and Morgan, 2009) deposited over much longer timescales
364 (*e.g.*, months to years). We prefer the terms aspergo deposit and pyrocloud deposit to the classic
365 "ejecta layer" proposed previously (Hildebrand and Boynton, 1990; Smit, 1999) because it
366 defines more precisely the KPB deposit stratigraphy (*e.g.*, there is also ejecta in the fireball
367 layer).

368 All of the spherules in the aspergo deposit and most of the spherules in the coarser
369 fraction of the pyrocloud deposit consist of rotational and agglutinated/irregular forms (*i.e.*, no
370 spheres) with abundant vesicles, unmelted inclusions, and schlieren (Fig. 5A-B), suggesting an
371 origin from molten materials. The morphologies observed indicate rotation during flight and
372 frequent collisions. The shapes preserved in these populations reveal that the Bond number and
373 the angular momentum were sufficient for the shapes to progress from spheres to oblong
374 ellipsoids and more evolved morphologies (ovoids, rods, dumbbells, teardrops, bowls, and discs;
375 see Fig. 3 and Fig. 4), implying that gravitational forces dominated over surface tension forces
376 (Elkins-Tanton et al., 2003; Stauffer and Butler, 2010; Butler et al., 2011; Baldwin et al., 2015).
377 Conversely, concave-convex contacts in numerous spherules at Gorgonilla Island (Fig. 4A-C)
378 suggest several droplets arrived at high temperatures at the depositional site before sinking in the
379 Pacific Ocean.

380 The totality of the spherules in the fireball layer and most of the spherules in the finer
381 portion of the pyrocloud deposit consist exclusively of spheres of dense glass, lacking unmelted
382 inclusions, vesicles, and schlieren (Fig. 4C), reflecting that collisions and rotation played no role
383 in the formation and distribution of these spherules, and suggesting an origin from condensed
384 materials. The absence of rotation indicates that the Bond number was close to zero (< 0.09),
385 implying that surface tension forces dominated over gravitational forces, and the angular
386 momentum was not large enough for the spheres to evolve to other morphologies (Elkins-Tanton
387 et al., 2003; Stauffer and Butler, 2010; Butler et al., 2011; Baldwin et al., 2015).

388

389 **6.2. Analysis of the weight of fractions/layers**

390 In order to obtain an estimate of the weight distribution of each morphological category
391 by size fraction, all impact spherules were considered spheres. Considering the average size of
392 each size fraction, an average radius was estimated, which was used to calculate (Eq. 2) the
393 volume (V) of an equivalent sphere and its respective weight according to a glass density value
394 of 2.7g cm⁻³. The values obtained are presented in Table S1. The Volume (V) is described in the
395 following equation:

$$396 \quad V = 4/3 \pi r^3 \quad (2)$$

397 Where π is a mathematical constant that is the ratio of a circle's circumference to its diameter,
398 approximately equal to 3.14159, and the variable r represents a sphere's radius (in cm).

399 The impact spherules from the aspergo deposit represent 95.015%, 54.132%, 37.854%,
400 and 37.796% of the weight of the KPB layer in Wahalak Creek, Tanis, Gorgonilla Island, and
401 Zumaia, respectively. On the other hand, the impact spherules from the pyrocloud deposit
402 represent 4.985%, 45.868%, 62.143%, and 60.193% of the weight of the KPB layer at Wahalak
403 Creek, Tanis, Gorgonilla Island, and Zumaia, respectively. The weight of the spherules from the
404 fireball layer in the sites where it was studied represented only 0.002% and 1.835% of the weight
405 of the KPB layer in Gorgonilla Island and Zumaia, respectively (Table S1).

406

407 **6.3. Implications for a global reconstruction of the ejecta dispersal**

408 From a morphological point of view, the absence of spheres and the abundance of
409 rotational and agglutinated/irregular forms present in the aspergo deposit are related to rotation
410 and frequent collisions between two or more spherules liquid enough to fuse or deform,
411 suggesting ballistic distribution (Fig. 6).

412 Molten and condensed materials coexisting in the pyrocloud deposit suggests the
413 expansion of a fast-moving, scorching, and turbulent cloud (the "pyrocloud"), transporting
414 melted and vaporized materials from the impact site (Fig. 6). The pyrocloud could reach distal
415 positions ($> 5,000$ km), agreeing with numerical models suggesting that this cloud could have
416 traveled up to 3 km/s after traversing 5,000 km from the impact site (Artemieva and Morgan,
417 2020). Spherules transported ballistically and by the lateral expansion of the pyrocloud could
418 reach the studied sites within a few minutes to a few hours after the impact and may be included
419 in tsunami or surge deposits in proximal to intermediate locations ($< 5,000$ km). The stratigraphic
420 record suggests that the catastrophic deposits triggered by the Chicxulub impact and the arrival
421 of molten spherules ejected from Chicxulub were coincident and took place during the first hours
422 after the impact (DePalma et al., 2019; Artemieva and Morgan, 2020; Senel et al., 2023;
423 LeVeque et al., 2024). The lack of spherules smaller than 0.3 mm at Wahalak Creek and Tanis
424 may imply that the high-energy deposits preserved there were deposited before the arrival of the
425 fireball layer spherules.

426 We interpret, as in previous works (Johnson and Melosh, 2012; Belza et al., 2017;
427 Goderis et al., 2021), that the spherules included in the fireball layer correspond to condensed
428 droplets from the Chicxulub impact-derived plume (Fig. 6) supporting the conclusions of
429 numerical models (Artemieva and Morgan, 2020). We did not find evidence (signs of rotation or
430 collisions between spherules) indicating that these materials could have reached distal areas
431 following ballistic trajectories or at high temperatures. The vapors included in the plume, rich in
432 shocked minerals and sediments enriched in platinum-group elements, may only have cooled
433 sufficiently over a few hours to days to allow condensation of the spherules (Toon et al., 2016),
434 and the settling of the distal ejecta should have taken years (Vellekoop et al., 2014; Goderis et

435 al., 2021) excluding the possibility of being included in the catastrophic deposits that
436 accumulated shortly after the Chicxulub impact. Condensation as the primary formation
437 mechanism for the fireball layer is also suggested by the exclusive occurrence of homogeneous
438 glass spherules in this layer (Fig 4C).

439

440 **7. Conclusions**

441 In this work, more than three thousand impact spherules directly related to the Chicxulub
442 impact have been investigated from a morphological and morphometric point of view. Impact
443 spherules were collected at the intermediate sites of Wahalak Creek and Tanis in the USA,
444 Gorgonilla Island in the Colombian Pacific, and the distal site of Zumaia, northern Spain. At the
445 time of the impact, these sites were located approximately 1,500 km north, 3,000 km north, 3,000
446 km south, and 7,000 km east of the Chicxulub crater, respectively.

447 The thorough analyses of the spherules by size range, morphological features, and internal
448 structure allowed us to define three distinct populations of impact spherules: 1) a coarser fraction
449 (aspergo deposit) containing rotational and agglutinated/irregular forms (size > 2mm) with
450 abundant vesicles, unmelted inclusions, and schlieren, implies an origin from molten materials,
451 rotation during flight and frequent collisions, that suggest a distribution mechanism following
452 ballistic trajectories: 2) an intermediate fraction (pyrocloud deposit) representing a mixture of
453 spheres, rotational, and agglutinated/irregular forms (size 0.3 - 2 mm), which morphology and
454 internal structure suggest the complex interaction of spherules of molten and condensed origin,
455 distributed by the expansion of a high-temperature turbulent cloud, and 3) a globally distributed
456 fireball layer composed entirely of spheres (size < 0.3 mm) condensed from the Chicxulub plume.

457 The importance of the fractions in thickness and volume/weight varies with distance from
458 the crater. The spherules' size and the deposits' thickness decrease with the distance from the
459 impact site. The aspergo deposit constitutes most of the total weight of the impact spherules in
460 the proximal sites, while the pyrocloud deposit represents most of the materials in the distal sites.
461 The weight of the fireball layer is not significant.

462 Our work offers the first evidence that ballistic trajectories and a "scorching dense cloud"
463 (the pyrocloud) reached Western Europe, *i.e.*, > 7,000 km from the Chicxulub crater during the
464 minutes and hours following the Chicxulub impact; however, future work is needed to fully assess
465 the extent of distribution of each of the proposed mechanisms.

466 Although the detailed study of Chicxulub impact spherule features (using three-
467 dimensional samples) provides physical evidence and a better understanding of the processes in
468 motion during massive asteroid impacts, it will be necessary to acquire and analyze more data
469 from sites at different positions from the crater, including proximal and ultra distal locations.

470 Further physical and numerical modeling and detailed geochemical analyses of the
471 different spherule types in other KPB sites around the globe might help us resolve how impact
472 spherules are formed and transported. Understanding these processes will have implications for
473 asteroid impacts on the Earth and other terrestrial planets with atmospheres.

474

475 **Acknowledgments**

476 We thank Parques Nacionales de Colombia for allowing access to Gorgona Island
477 National Park and Paleoexplorer SAS for financial support. Gavin Kenny and Vivi Vajda are
478 thanked for their assistance with SEM analyses. Reviews and comments by Joanna Morgan and
479 Billy Glass provided helpful suggestions for improving early versions of this manuscript. We

480 thank Reinaldo Rojas, Sean Gulick, and James Witts for their helpful comments and suggestions,
481 which greatly improved the quality of this manuscript. HB acknowledges the support provided
482 by the Geological Society of America 2022 Graduate Student Research Grant and the
483 International Association of Sedimentologists 2023 Postgraduate Grant Scheme. HB, MDP, and
484 YC acknowledge the support provided by NSF grant EAR-2002370. This research is part of the
485 grants PID2022-136233NB-I00 funded by MCIN/AEI/10.13039/501100011033 and by ERDF A
486 way of making Europe, and DGA group E33_23R funded by the Aragonese Government and by
487 ERDF A way of making Europe. VG acknowledges support from Ministerio de Universidades
488 (MIU) and the European Union (Margarita Salas post-doctoral grant) funded by the European
489 Union-NextGeneration EU. We acknowledge the use of the Servicio General de Apoyo a la
490 Investigación-SAI, Universidad de Zaragoza, Spain, for providing scanning electron microscope
491 micrographs.

492

493 **CRedit authorship contribution statement**

494 **Hermann D. Bermúdez:** Conceptualization, Funding acquisition, Investigation,
495 Methodology, Visualization, Writing – original draft, Writing – review and editing. **Liliana**
496 **Bolívar:** Conceptualization, Funding acquisition, Investigation, Methodology, Writing – review
497 and editing. **José A. Arz:** Investigation, Writing - review & editing. **Ignacio Arenillas:**
498 Investigation, Writing - review & editing. **Vicente Gilabert:** Investigation, Writing - review &
499 editing, **Robert DePalma:** Investigation, Writing - review & editing, **George Phillips;**
500 Investigation, Writing -review & editing, **Maurizia De Palma:** Methodology. **Daniela**
501 **Bermúdez:** Methodology, Investigation. **Clemencia Gómez:** Supervision. **Ying Cui:**
502 Supervision, Writing - review & editing.

503

504 **Declaration of competing interest**

505 The authors declare that they have no known competing financial interests or personal
506 relationships that could have appeared to influence the work reported in this paper.

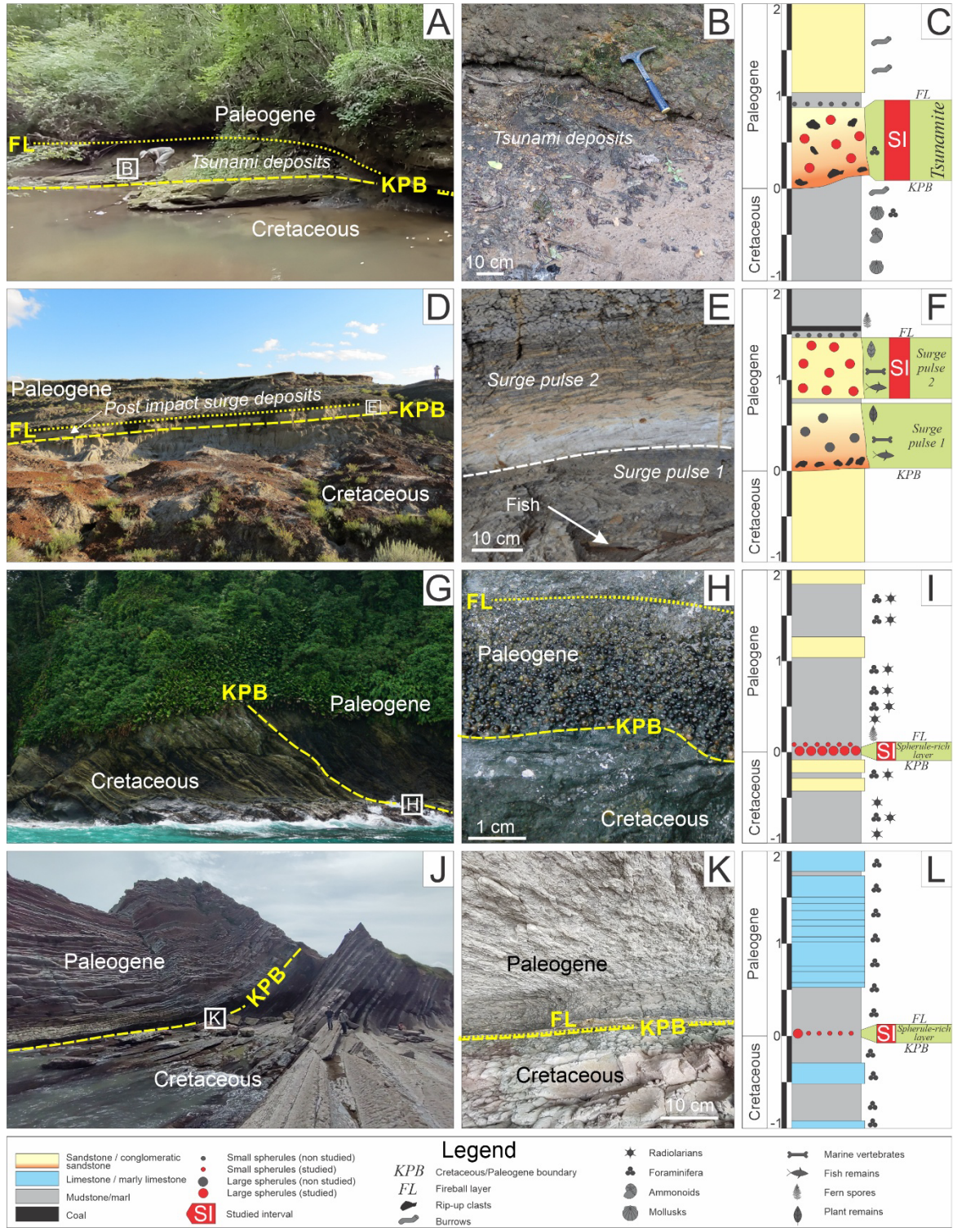
507 **Figure captions**



508

509 Fig. 1. Paleogeographic map for the KPB (Scotese, 2021) showing the locations of the studied

510 sites.

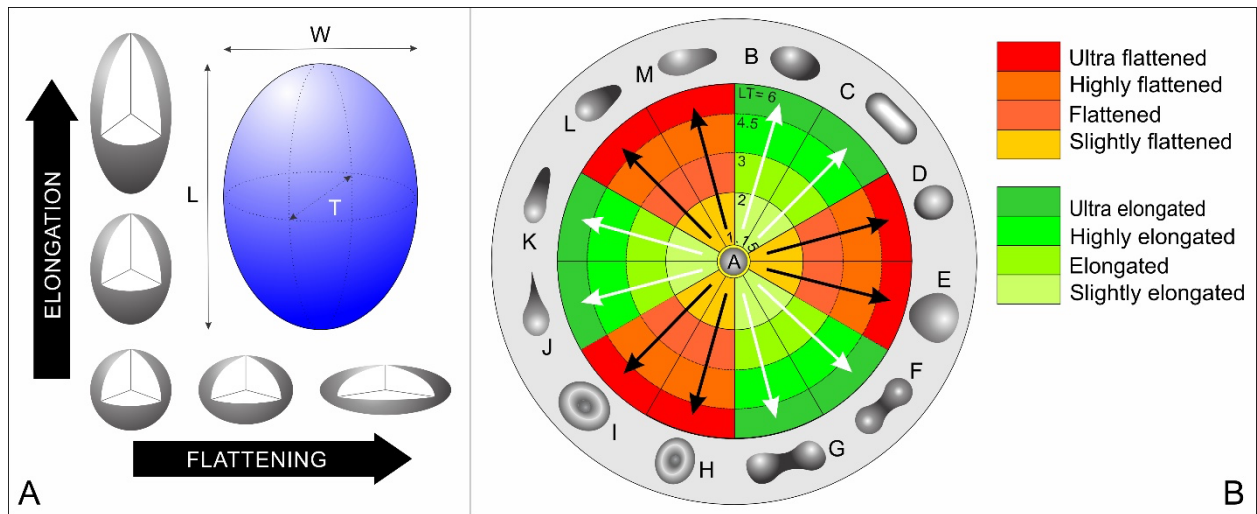


511

512 Fig. 2. Representative field photos (outcrop/detail) and stratigraphic column of the KPBC sections

513 in Wahalak Creek (A-C), Tanis (D-F), Gorgonilla Island (G-I), and Zumaia (J-L). For the

514 stratigraphic section the scale is in meters.



515

516 Fig. 3. A) Geometric parameters used to define ellipsoids: L = major axis, W = intermediate axis,

517 T = thickness. The L/W ratio defines elongation. The W/T ratio defines flattening. B) New

518 classification scheme for splash-form impact spherules. A= Spheres; B= Ovoids; C= Rods; D=

519 Ovoid disks; E= Spherical disks; F= Dumbbells; G= Flattened dumbbells; H= Oval bowls; I=

520 Circular bowls; J= Teardrops; K= Elongated teardrops; L= Ovoid teardrops; M= Flattened

521 teardrops. The numbers represent values of the L/W ratio for elongation (green sectors and white

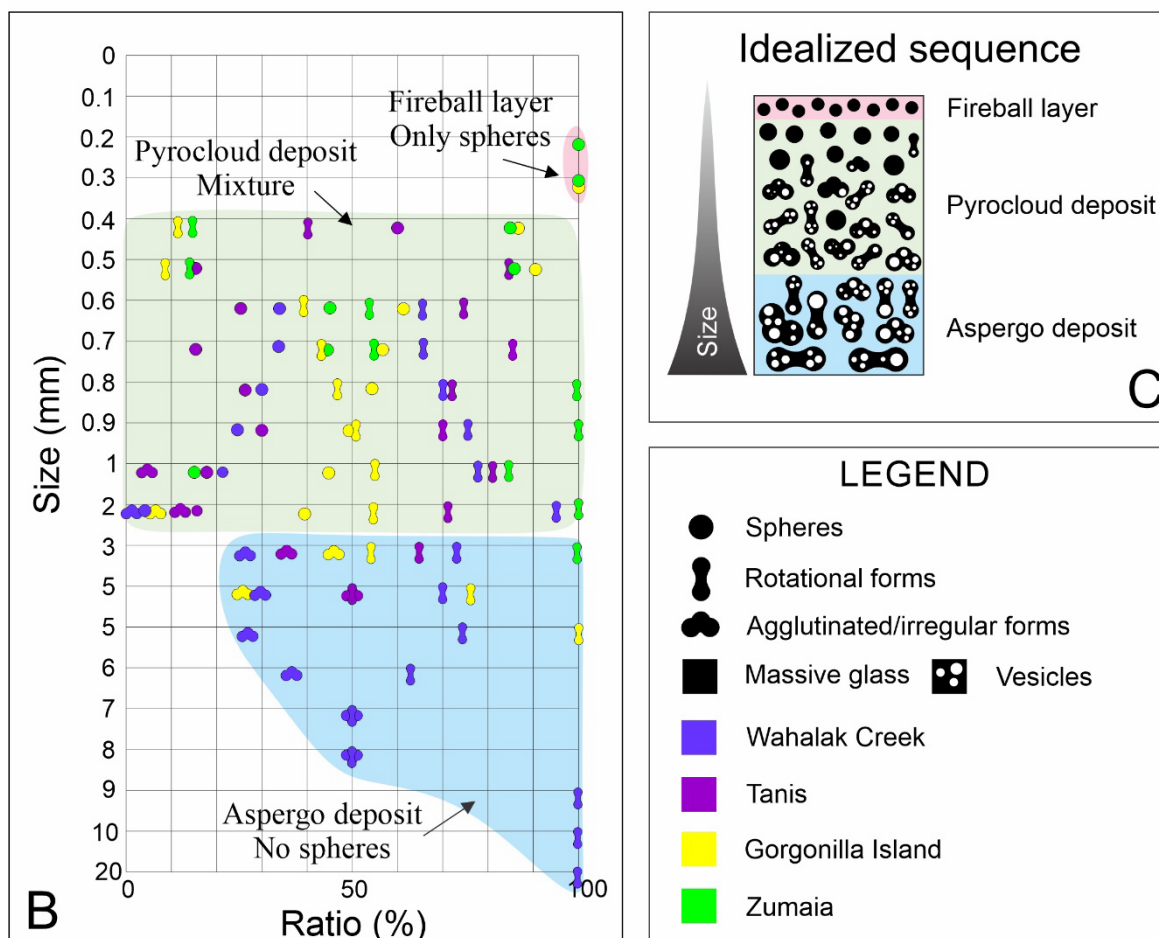
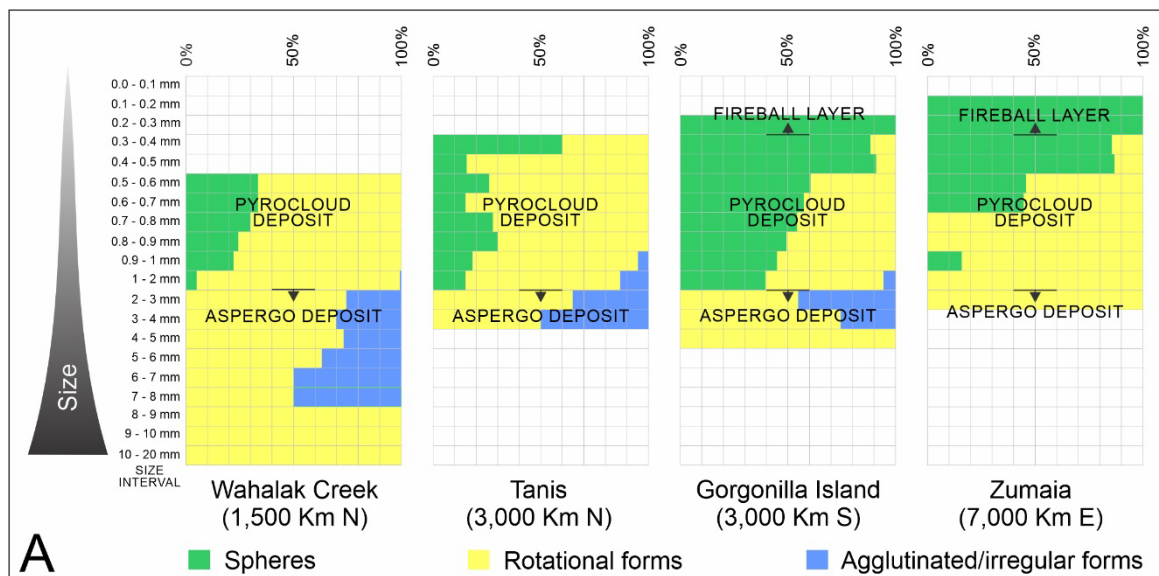
522 arrows) and the W/T ratio for flattening (orange sectors and black arrows).

523



524

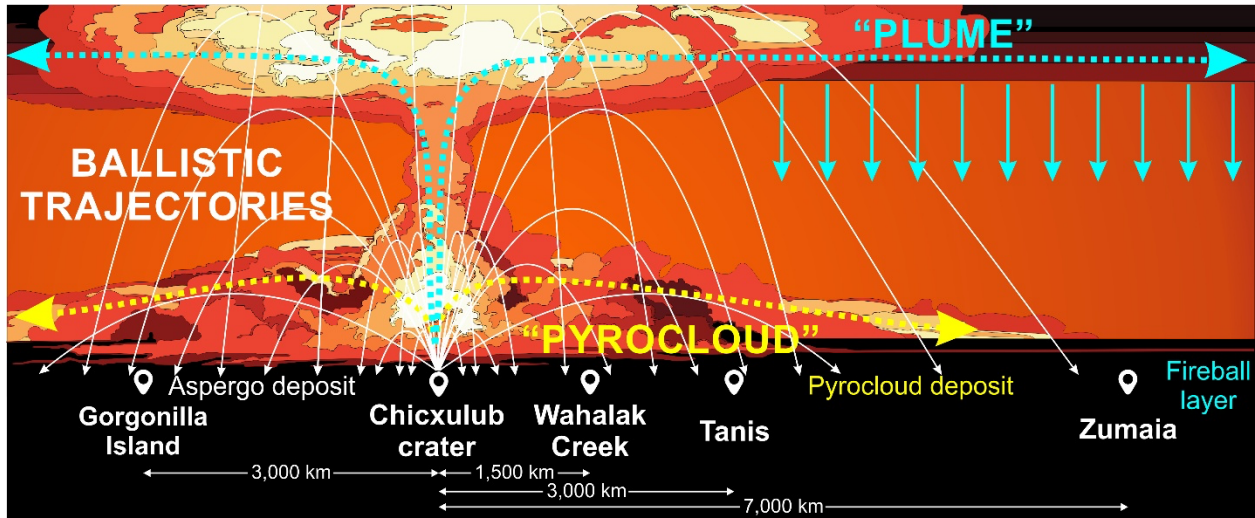
525 Fig. 4. Selected Chicxulub impact spherules. A-C) Backscattered electron images of typical
 526 spherules from Gorgonilla Island showing concave-convex contacts (white lines). A) Bottom of
 527 the KP bed. B) Middle part of the KP bed. C) Top of the KP bed. D) Zumaia (including 5
 528 Backscattered electron images on the right). E) Tanis. F) Gorgonilla Island (left: reflected light;
 529 right: transmitted light). G) Wahalak Creek.



530

531 Fig. 5. Percent distribution of impact spherules by morphology and size. A) Results by site. B)

532 Combined results. C) Idealized KPBed sequence.



533

534 Fig. 6. Conceptual model of distribution mechanisms of molten and vaporized materials expelled
 535 after the Chicxulub impact (not to scale).

536

537 **Supplemental Material.** Supplementary Table S1 (in a separate supplementary data file named
 538 Table S1_Bermudez_et_al.xlsx.).

539 **References**

- 540 Arenillas, I., Arz, J.A., Grajales-Nishimura, J.M., Murillo-Muñetón, G., Alvarez, W., Camargo-
541 Zanoguera, A., Molina, E., and Rosales-Domínguez, C., 2006, Chicxulub impact event is
542 Cretaceous/Paleogene boundary in age: New micropaleontological evidence: Earth and
543 Planetary Science Letters, v. 249, p. 241–257, <https://doi.org/10.1016/j.epsl.2006.07.020>
- 544 Arz, J.A., Arenillas, I., Soria, A.R., Alegret, L., Grajales-Nishimura, J.M., Liesa, C.L.,
545 Meléndez, A., Molina, E., and Rosales, M.C., 2001, Micropaleontology and
546 Sedimentology of the Cretaceous/Paleogene boundary at La Ceiba (Mexico): impact-
547 generated sediment gravity flows. *Journal of South American Earth Sciences*, v. 14, no 5,
548 p. 505-519, [https://doi.org/10.1016/S0895-9811\(01\)00049-9](https://doi.org/10.1016/S0895-9811(01)00049-9)
- 549 Arz, J.A., Alegret, L., and Arenillas, I., 2004, Foraminiferal biostratigraphy and
550 paleoenvironmental reconstruction at Yaxcopoil-1 drill hole (Chicxulub crater, Yucatan
551 Peninsula). *Meteoritics & Planetary Science*, v. 39, no 7, p. 1099-1111,
552 <https://doi.org/10.1111/j.1945-5100.2004.tb01131.x>
- 553 Arz, J.A., Arenillas, I., Grajales-Nishimura, J.M., Liesa, C.L., Soria, A.R., Rojas, R., Calmus, T.,
554 and Gilabert, V., 2022, No evidence of multiple impact scenario across the
555 Cretaceous/Paleogene boundary based on planktic foraminiferal biochronology, in
556 Koeberl, C., Claeys, P., and Montanari, A., eds., *From the Guajira Desert to the*
557 *Apennines, and from Mediterranean Microplates to the Mexican Killer Asteroid:*
558 *Honoring the Career of Walter Alvarez: Geological Society of America Special Paper*, v.
559 557, p. 415-448, [https://doi.org/10.1130/2022.2557\(20\)](https://doi.org/10.1130/2022.2557(20))
- 560 Artemieva, N., and Morgan, J. V., 2009, Modeling the formation of the K–Pg boundary layer:
561 *Icarus*, v. 201, no. 2, p. 768-780, <https://doi.org/10.1016/j.icarus.2009.01.021>

562 Artemieva, N., and Morgan, J. V., 2020, Global K-Pg layer deposited from a dust cloud:
563 Geophysical Research Letters, v. 47, no. 6, p. e2019GL086562,
564 <https://doi.org/10.1029/2019GL086562>

565 Artemieva, N., Morgan, J. V., and Expedition 364 Science Party., 2017, Quantifying the release
566 of climate-active gases by large meteorite impacts with a case study of Chicxulub:
567 Geophysical Research Letters, v. 44, no. 20, p. 10,180-110,188,
568 <https://doi.org/10.1002/2017GL074879>

569 Baldwin, K. A., Butler, S. L., and Hill, R. J., 2015, Artificial tektites: an experimental technique
570 for capturing the shapes of spinning drops: Scientific reports, v. 5, no. 1, p. 1-5,
571 <https://doi.org/10.1038/srep07660>

572 Belza, J., Goderis, S., Montanari, A., Vanhaecke, F., and Claeys, P., 2017, Petrography and
573 geochemistry of distal spherules from the K–Pg boundary in the Umbria–Marche region
574 (Italy) and their origin as fractional condensates and melts in the Chicxulub impact
575 plume: *Geochimica et Cosmochimica Acta*, v. 202, p. 231-263,
576 <https://doi.org/10.1016/j.gca.2016.12.018>

577 Bermudez, H. D., Arenillas, I., Arz, J. A., Vajda, V., Renne, P. R., Gilabert, V., and Rodríguez,
578 J. V., 2018, The Cretaceous/Paleogene boundary deposits on Gorgonilla Island: The
579 Geology of Colombia, v. 3, p. 1-34, <https://doi.org/10.32685/pub.esp.37.2019.01>

580 Bermúdez, H. D., García, J., Stinnesbeck, W., Keller, G., Rodríguez, J. V., Hanel, M., Hopp, J.,
581 Schwarz, W. H., Trieloff, M., and Bolívar, L., 2016, The Cretaceous–Palaeogene
582 boundary at Gorgonilla Island, Colombia, South America: *Terra Nova*, v. 28, no. 1, p. 83-
583 90, <https://doi.org/10.1111/ter.12196>

584 Beyer, H., 1962, *Philippine Tektites*, Vol. 1 Part 2: Manila: University of The Philippines.

585 Bohor, B. F., 1990, Shocked quartz and more: Impact signatures in Cretaceous/Tertiary
586 boundary clays: Geological Society of America Special Papers, v. 247, p. 335-342.

587 Bralower, T. J., Paull, C. K., and Mark Leckie, R., 1998, The Cretaceous-Tertiary boundary
588 cocktail: Chicxulub impact triggers margin collapse and extensive sediment gravity
589 flows: *Geology*, v. 26, no. 4, p. 331-334, [https://doi.org/10.1130/0091-](https://doi.org/10.1130/0091-7613(1998)026<0331:TCTBCC>2.3.CO;2)
590 [7613\(1998\)026<0331:TCTBCC>2.3.CO;2](https://doi.org/10.1130/0091-7613(1998)026<0331:TCTBCC>2.3.CO;2)

591 Butler, S., Stauffer, M., Sinha, G., Lilly, A., and Spiteri, R., 2011, The shape distribution of
592 splash-form tektites predicted by numerical simulations of rotating fluid drops: *Journal of*
593 *fluid mechanics*, v. 667, p. 358-368, <https://doi.org/10.1017/S0022112010005641>

594 Chiarenza, A. A., and Brusatte, S. L., 2023, *Dinosaurs, Extinction Theories for, Reference*
595 *Module in Life Sciences*, Elsevier.

596 Christeson, G. L., Morgan, J. V., and Gulick, S. P. S., 2021, Mapping the Chicxulub Impact
597 Stratigraphy and Peak Ring Using Drilling and Seismic Data: *Journal of Geophysical*
598 *Research: Planets*, v. 126, no. 8, p. e2021JE006938.

599 Claeys, P., Kiessling, W., Alvarez, W., Koeberl, C., and MacLeod, K., 2002, Distribution of
600 Chicxulub ejecta at the Cretaceous-Tertiary boundary: *Special Papers-Geological Society*
601 *of America*, p. 55-68.

602 Denne, R. A., Scott, E. D., Eickhoff, D. P., Kaiser, J. S., Hill, R. J., and Spaw, J. M., 2013,
603 Massive Cretaceous-Paleogene boundary deposit, deep-water Gulf of Mexico: New
604 evidence for widespread Chicxulub-induced slope failure: *Geology*, v. 41, no. 9, p. 983-
605 986.

606 DePalma, R. A., Smit, J., Burnham, D. A., Kuiper, K., Manning, P. L., Oleinik, A., Larson, P.,
607 Maurrasse, F. J., Vellekoop, J., Richards, M. A., Gurche, L., and Alvarez, W., 2019, A

608 seismically induced onshore surge deposit at the KPg boundary, North Dakota:
609 Proceedings of the National Academy of Sciences, v. 116, no. 17, p. 8190-8199,
610 <https://doi.org/10.1073/pnas.1817407116>

611 Elkins Tanton, L., Kelly, D., Bico, J., and Bush, J., 2002, Microtektites as vapor condensates,
612 and a possible new strewn field at 5 Ma, in Proceedings Lunar and Planetary Science
613 Conference XXXIII (2002), p. 1622.

614 Elkins-Tanton, L. T., Aussillous, P., Bico, J., Quere, D., and Bush, J. W., 2003, A laboratory
615 model of splash-form tektites: Meteoritics & Planetary Science, v. 38, no. 9, p. 1331-
616 1340, <https://doi.org/10.1111/j.1945-5100.2003.tb00317.x>

617 Glass, B. P., 2016, Glass: The geologic connection: International Journal of Applied Glass
618 Science, v. 7, no. 4, p. 435-445.

619 Glass, B., and Burns, C. A., 1988, Microkrystites-A new term for impact-produced glassy
620 spherules containing primary crystallites, in Proceedings IN: Lunar and Planetary Science
621 Conference, 18th, Houston, TX, Mar. 16-20, 1987, Proceedings (A89-10851 01-91).
622 Cambridge and New York/Houston, TX, Cambridge University Press/Lunar and
623 Planetary Institute, p. 455-458.1988, Volume 18, p. 455-458.

624 Glass, B. P., and Simonson, B. M., 2011, Variation in Distal Impact Ejecta with Distance from
625 the Source Crater: A Model: Meteoritics and Planetary Science Supplement, v. 74, p.
626 5035.

627 Glass, B. P., and Simonson, B. M., 2012, Distal impact ejecta layers: Spherules and more:
628 Elements, v. 8, no. 1, p. 43-48, <https://doi.org/10.2113/gselements.8.1.43>

629 Glass, B. P., and Simonson, B. M., 2013, Distal impact ejecta layers: A record of large impacts
630 in sedimentary deposits, Springer Science & Business Media.

631 Gilabert, V., Batenburg, S. J., Arenillas, I., and Arz, J. A., 2022, Contribution of orbital forcing
632 and Deccan volcanism to global climatic and biotic changes across the Cretaceous-
633 Paleogene boundary at Zumaia, Spain: *Geology*, v. 50, no. 1, p. 21-25,
634 <https://doi.org/10.1130/G49214.1>

635 Goderis, S., Sato, H., Ferrière, L., Schmitz, B., Burney, D., Kaskes, P., Vellekoop, J., Wittmann,
636 A., Schulz, T., Chernonozhkin, S. M., Claeys, P., de Graaff, S. J., Déhais, T., de Winter,
637 N. J., Elfman, M., Feignon, J. G., Ishikawa, A., Koeberl, K., Kristiansson, P., Neal, C. R.,
638 Owens, J. D., Schmieder, M., Sinnesael, M., Vanhaecke, F., Van Malderen, S. J. M.,
639 Bralower, T. J., Gulick, S.P., Kring, D. A., Lowery, C. M., Morgan, J. V, Smit, J.,
640 Whalen, M. T., and IODP-ICDP Expedition 364 Scientists., 2021, Globally distributed
641 iridium layer preserved within the Chicxulub impact structure: *Science advances*, v. 7,
642 no. 9, p. eabe3647, <https://doi.org/10.1126/sciadv.abe3647>

643 Gulick, S. P., Bralower, T. J., Ormö, J., Hall, B., Grice, K., Schaefer, B., Lyons, S., Freeman, K.
644 H., Morgan, J. V., and Artemieva, N., 2019, The first day of the Cenozoic: *Proceedings*
645 *of the National Academy of Sciences*, v. 116, no. 39, p. 19342-19351. Hildebrand, A. R.,
646 and Boynton, W. V., 1990, Proximal Cretaceous-Tertiary Boundary Impact Deposits in
647 the Caribbean: *Science*, v. 248, no. 4957, p. 843-847,
648 <https://doi.org/10.1126/science.248.4957.84>

649 Gulick, S. P. S., 2025, *End of the Cretaceous*: Geological Society, London, Special Publications,
650 v. 544, no. 1, p. SP544-2023-2176.

651 Hildebrand, A. R., and Boynton, W. V., 1990, Proximal Cretaceous-Tertiary Boundary Impact
652 Deposits in the Caribbean: *Science*, v. 248, no. 4957, p. 843-847.

653 Hildebrand, A. R., Penfield, G. T., Kring, D. A., Pilkington, M., Camargo Z, A., Jacobsen, S. B.,
654 and Boynton, W. V., 1991, Chicxulub crater: a possible Cretaceous/Tertiary boundary
655 impact crater on the Yucatan Peninsula, Mexico: *Geology*, v. 19, no. 9, p. 867-871.

656 Johnson, B. C., and Melosh, H. J., 2012, Formation of spherules in impact produced vapor
657 plumes: *Icarus*, v. 217, no. 1, p. 416-430, <https://doi.org/10.1016/j.icarus.2011.11.020>

658 Koeberl, C., 1986, Geochemistry of tektites and impact glasses: *Annual Review of Earth and*
659 *Planetary Sciences*, v. 14, no. 1, p. 323-350.

660 Koeberl, C., 2002, Mineralogical and geochemical aspects of impact craters: *Mineralogical*
661 *Magazine*, v. 66, no. 5, p. 745-768.

662 Kring, D. A., and Durda, D. D., 2002, Trajectories and distribution of material ejected from the
663 Chicxulub impact crater: Implications for postimpact wildfires: *Journal of Geophysical*
664 *Research: Planets*, v. 107, no. E8, p. 6-1-6-22, <https://doi.org/10.1029/2001JE001532>

665 Larina, E., Garb, M., Landman, N., Dastas, N., Thibault, N., Edwards, L., Phillips, G., Rovelli,
666 R., Myers, C., and Naujokaityte, J., 2016, Upper Maastrichtian ammonite biostratigraphy
667 of the Gulf Coastal Plain (Mississippi Embayment, southern USA): *Cretaceous Research*,
668 v. 60, p. 128-151.

669 LeVeque, R. J., DePalma, R. A., Garrison-Laney, C., Maurya, S., Smit, J., and Richards, M. A.,
670 2024, Possible Mechanisms for Tsunami-Like Surge Deposits Due To the Chicxulub
671 Impact at the K-Pg Boundary at the Tanis Site, North Dakota: *Journal of Geophysical*
672 *Research: Solid Earth*, v. 129, no. 5, p. e2023JB027643.

673 Melosh, H. J., 1989, *Impact cratering: A geologic process*: New York: Oxford University Press;
674 Oxford: Clarendon Press.

675 Molina, E., Alegret, L., Arenillas, I., Arz, J.A., Gallala, N., Hardenbol, J., von Salis, K.,
676 Steurbaut, E., Vandenberghe, N., and Zaghbib-Turki, D., 2006, The global boundary
677 stratotype section and point for the base of the Danian stage (Paleocene, Paleogene,
678 "Tertiary," Cenozoic) at El Kef, Tunisia - Original definition and revision. *Episodes*, v.
679 29, no. 4, p. 263-273, <https://doi.org/10.18814/epiiugs/2006/v29i4/004>

680 Molina, E., Alegret, L., Arenillas, I., Arz, J. A., Gallala, N., Grajales-Nishimura, J. M., Murillo-
681 Muñetón, G., and Zaghbib-Turki, D., 2009, The Global Boundary Stratotype Section and
682 Point for the base of the Danian Stage (Paleocene, Paleogene, "Tertiary", Cenozoic):
683 Auxiliary sections and correlation: *Episodes*, v. 32, p. 84–95,
684 <https://doi.org/10.18814/epiiugs/2009/v32i2/002>.

685 Montanari, A., and Koeberl, C., 2000, *Impact stratigraphy: the Italian record*, Springer Science &
686 Business Media.

687 Morgan, J. V., Bralower, T. J., Brugger, J., and Wünnemann, K., 2022, The Chicxulub impact
688 and its environmental consequences: *Nature Reviews Earth & Environment*, v. 3, no. 5,
689 p. 338-354, <https://doi.org/10.1038/s43017-022-00283-y>

690 Osinski, G. R., Grieve, R. A. F., Ferrière, L., Losiak, A., Pickersgill, A. E., Cavosie, A. J.,
691 Hibbard, S. M., Hill, P. J. A., Bermudez, J. J., Marion, C. L., Newman, J. D., and
692 Simpson, S. L., 2022, Impact Earth: A review of the terrestrial impact record: *Earth-*
693 *Science Reviews*, v. 232, p. 104112, <https://doi.org/10.1016/j.earscirev.2022.104112>

694 Pierazzo, E., and Artemieva, N., 2012, Local and global environmental effects of impacts on
695 Earth: *Elements*, v. 8, no. 1, p. 55-60.

696 Reihart, J. S., 1958, Impact effects and tektites: *Geochimica et Cosmochimica Acta*, v. 14, no. 4,
697 p. 287-290.

698 Renne, P. R., Arenillas, I., Arz, J. A., Vajda, V., Gilabert, V., and Bermúdez, H. D., 2018, Multi-
699 proxy record of the Chicxulub impact at the Cretaceous-Paleogene boundary from
700 Gorgonilla Island, Colombia: *Geology*, v. 46, no. 6, p. 547-550,
701 <https://doi.org/10.1130/G40224.1>

702 Sanford, J. C., Snedden, J. W., and Gulick, S. P. S., 2016, The Cretaceous-Paleogene boundary
703 deposit in the Gulf of Mexico: Large-scale oceanic basin response to the Chicxulub
704 impact: *Journal of Geophysical Research: Solid Earth*, v. 121, no. 3, p. 1240-1261.

705 Schmieder, M., and Kring, D. A., 2020, Earth's impact events through geologic time: a list of
706 recommended ages for terrestrial impact structures and deposits: *Astrobiology*, v. 20, no.
707 1, p. 91-141.

708 Schulte, P., Deutsch, A., Salge, T., Berndt, J., Kontny, A., MacLeod, K., Neuser, R., and
709 Krumm, S., 2009, A dual-layer Chicxulub ejecta sequence with shocked carbonates from
710 the Cretaceous–Paleogene (K–Pg) boundary, Demerara Rise, western Atlantic:
711 *Geochimica et Cosmochimica Acta*, v. 73, no. 4, p. 1180-1204.

712 Schulte, P., Schulte, P., Alegret, L., Arenillas, I., Arz, J. A., Barton, P. J., Bown, P. R., Bralower,
713 T. J., Christeson, G. L., Claeys, P., Cockell, C. S., Collins, G. S., Deutsch, A., Goldin, T.
714 J., Goto, K., Grajales-Nishimura, J. M., Grieve, R. A. F., Gulick, S. P. S., Johnson, K. R.,
715 Kiessling, W., Koeberl, C., Kring, D. A., MacLeod, K. G., Matsui, T., Melosh, J.,
716 Montanari, A., Morgan, J. V., Neal, C.R., Nichols, D.J., Norris, R.D., Pierazzo, E.,
717 Ravizza, G., Rebolledo-Vieyra, M., Reimold, W.U., Robin, E., Salge, T., Speijer, R.P.,
718 Sweet, A.R., Urrutia-Fucugauchi, J., Vajda, V., Whalen, M.T., Willumsen, P.S., 2010,
719 The Chicxulub asteroid impact and mass extinction at the Cretaceous-Paleogene

720 boundary: *Science*, v. 327, no. 5970, p. 1214-1218,
721 <https://doi.org/10.1126/science.1177265>

722 Scotese, C. R., 2021, An Atlas of Phanerozoic Paleogeographic Maps: The Seas Come In and the
723 Seas Go Out: *Annual Review of Earth and Planetary Sciences*, v. 49, no. 1, p. 679-728,
724 <https://doi.org/10.1146/annurev-earth-081320-064052>

725 Senel, C. B., Kaskes, P., Temel, O., Vellekoop, J., Goderis, S., DePalma, R., Prins, M. A.,
726 Claey's, P., and Karatekin, Ö., 2023, Chicxulub impact winter sustained by fine silicate
727 dust: *Nature Geoscience*, 16, 1033–1040, <https://doi.org/10.1038/s41561-023-01290-4>

728 Simonson, B. M., and Glass, B. P., 2004, Spherule layers—Records of ancient impacts: *Annu.*
729 *Rev. Earth Planet. Sci.*, v. 32, p. 329-361,
730 <https://doi.org/10.1146/annurev.earth.32.101802.120458>

731 Smit, J., 1999, The global stratigraphy of the Cretaceous-Tertiary boundary impact ejecta:
732 *Annual Review of Earth and Planetary Sciences*, v. 27, no. 1, p. 75-113,
733 <https://doi.org/10.1146/annurev.earth.27.1.75>

734 Soria, A.R., Liesa, C.L., Mata, M.P., Arz, J.A., Alegret, L., Arenillas, I., and Melendez, A.,
735 2001, Slumping and a sandbar deposit at the Cretaceous-Tertiary boundary in the El
736 Tecolote section (northeastern Mexico): An impact-induced sediment gravity flow:
737 *Geology*, v. 29, p. 231-234,
738 [https://doi.org/10.1130/00917613\(2001\)029<0231:SAASDA>2.0.CO;2](https://doi.org/10.1130/00917613(2001)029<0231:SAASDA>2.0.CO;2).

739 Sosa-Montes de Oca, C., Witts, J. D., Lowery, C. M., Kearns, L. E., Garb, M. P., Naujokaityte,
740 J., Myers, C. E., Landman, N. H., and Pancost, R. D., 2024, Intense Changes in the Main
741 Source of Organic Carbon to the Gulf Coastal Plain Following the Cretaceous-Paleogene
742 Boundary: *Paleoceanography and Paleoclimatology*, v. 39, no. 8, p. e2024PA004887.

743 Stauffer, M. R., and Butler, S. L., 2010, The shapes of splash-form tektites: their geometrical
744 analysis, classification and mechanics of formation: *Earth, Moon, and Planets*, v. 107, no.
745 2-4, p. 169-196, <https://doi.org/10.1007/s11038-010-9359-y>

746 Suess, F. E., 1900, *Die Herkunft der Moldavite und verwandter Gläser*, Geologischen
747 Reichsanstalt.

748 Toon, O. B., Bardeen, C., and Garcia, R., 2016, Designing global climate and atmospheric
749 chemistry simulations for 1 and 10 km diameter asteroid impacts using the properties of
750 ejecta from the K-Pg impact: *Atmospheric Chemistry and Physics*, v. 16, no. 20, p.
751 13185-13212, <https://doi.org/10.5194/acp-16-13185-2016>

752 Vajda, V., and Bercovici, A., 2014, The global vegetation pattern across the Cretaceous–
753 Paleogene mass extinction interval: A template for other extinction events: *Global and
754 Planetary Change*, v. 122, p. 29-49.

755 Vellekoop, J., Sluijs, A., Smit, J., Schouten, S., Weijers, J. W., Damsté, J. S. S., and Brinkhuis,
756 H., 2014, Rapid short-term cooling following the Chicxulub impact at the Cretaceous–
757 Paleogene boundary: *Proceedings of the National Academy of Sciences*, v. 111, no. 21, p.
758 7537-7541, <https://doi.org/10.1073/pnas.1319253111>

759 Witts, J. D., Landman, N. H., Garb, M. P., Boas, C., Larina, E., Rovelli, R., Edwards, L. E.,
760 Sherrell, R. M., and Cochran, J. K., 2018, A fossiliferous spherule-rich bed at the
761 Cretaceous–Paleogene (K–Pg) boundary in Mississippi, USA: implications for the K–Pg
762 mass extinction event in the Mississippi Embayment and Eastern Gulf Coastal Plain:
763 *Cretaceous Research*, v. 91, p. 147-167, <https://doi.org/10.1016/j.cretres.2018.06.002>